

Classical stationary particle distributions in collision processes

Inés Samengo, R G Pregliasco and R O Barrachina

Centro Atómico Bariloche and Instituto Balseiro†, 8400 SC de Bariloche, Río Negro, Argentina‡

Received 24 November 1998

Abstract. We study the classical distribution of particles in a collision process. This is the classical analogue to the square modulus of the quantum mechanical stationary continuum wavefunction. We evaluate this distribution in coordinate and momentum space analytically, comparing its similarities and discrepancies with the corresponding quantum mechanical particle density.

1. Introduction

Since the pioneering work of Ford and Wheeler (1959a, b) and later, of Gryzinski (1965), the classical and semiclassical descriptions of scattering processes have provided deep insight into the physics of atomic collisions. Even nowadays, these theories often give a simple and accurate explanation of complex many-body phenomena involving non-elastic channels (see, for example, Swenson and Burgdörfer 1991, Reinhold *et al* 1991).

In a semiclassical approach, the asymptotic behaviour of the scattering continuum wavefunction is obtained from the classical deflection function $b(\Theta)$, relating the impact parameter b to the final deflection angle Θ (Ford and Wheeler 1959a, McDowell and Coleman 1970, Berry and Mount 1972, Brink 1985). Thus, the calculation of the semiclassical scattering cross section is not a difficult task, at least when compared with the full quantum mechanical procedure. However, in some cases it is important to know the particle density throughout the whole space, not just at infinity. For spherically symmetrical potentials, the WKB method provides a way to calculate the partial radial wavefunctions. The drawback is that the conditions of validity of this method usually imply that a very large number of partial waves have to be considered. In practical cases, this usually becomes discouragingly cumbersome. Besides, the full three-dimensional semiclassical approach requires the solution of the Hamilton–Jacobi equation, which is nonlinear and involves partial derivatives (Gutzwiller 1967, Berry and Mount 1972). In consequence, the semiclassical approach does not provide any computational advantage over the quantum mechanical solution of the Schrödinger equation.

On the other hand, the calculation of the classical distribution of particles in a collision process is a much simpler task. In this paper, we present a general and analytical method to evaluate the density of particles in coordinate and in momentum spaces. In a general situation, the relevant distribution ought to be calculated in the six-dimensional phase space by solving the Liouville equation (Goldstein 1959, Landau and Lifshitz 1976), eventually involving a time dependence. However, a stationary description of the scattering process allows one to write down the density in coordinate and momentum spaces, separately. We derive a general

† Comisión Nacional de Energía Atómica and Universidad Nacional de Cuyo, Argentina.

‡ Also members of the Consejo Nacional de Investigaciones Científicas y Técnicas.

method to carry out such a calculation for any spherically symmetric potential. Surprisingly enough, this result has not been considered before. Previous calculations (Rowe 1987) are special cases of our derivation.

Our proposal is to provide a classical analogue to the standard stationary presentation of collision theory. Instead of analysing the trajectories travelled by single particles, and relating a final deflection angle to an initial impact parameter, we calculate the particle distribution throughout the whole space. This is the classical counterpart to solving the time-independent Schrödinger equation. Studying the asymptotic behaviour of the particle density, the scattering cross section can be obtained following the same line of reasoning as the standard presentation of quantum mechanics (Fiol *et al* 1997).

The classical distribution of particles associated to a collision process is simply related to the accumulation or separation of trajectories. Therefore, whenever the classical and the quantum mechanical densities show similar structures, they can be explained as arising from causal Newtonian effects. On the other hand, if qualitative differences are found, there is certainty that an intrinsically quantum mechanical effect is showing up, as for instance an interference, diffraction or exchange phenomenon. This kind of comparison between the classical and the quantum mechanical distributions has been highly successful in the study of bound states of the hydrogen atom (Fock 1935, Pitaevskii 1962, Mapleton 1966, Samengo 1998a). In this paper we give the first derivation concerning collision processes in any central potential field.

In the following section we present the method for calculating the particle distribution in terms of the trajectories, in coordinate (section 2) and momentum space (section 3). We exemplify our method by applying it to the dipolar interaction $V(r) \propto 1/r^2$, the rigid sphere (in section 4) and the Coulomb potential (in section 5), for the attractive and repulsive cases. Finally, section 6 summarizes the main conclusions of this work.

2. Classical particle density

In this section we calculate the classical distribution of particles in a scattering process. Let us consider the situation shown in figure 1. An uniform flux j of particles of mass m and momentum p_0 collides with a force centre of potential energy $V(r)$. Very far away from this force centre, the trajectory of any given particle reads

$$r_0(t) = b + \frac{p_0}{m}t \quad (1)$$

with b the impact parameter. The number of particles δN that crosses an area element $\delta A = b \delta b \delta \phi$ in an interval δt long before the collision is $\delta N = j \delta A \delta t = j b \delta b \delta \phi \delta t$. These particles occupy the volume $\delta V_0 = (p_0/m) \delta A \delta t$. Therefore, the density at infinity

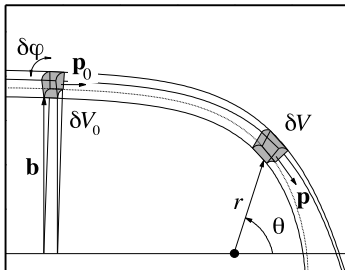


Figure 1. We select a group of δN particles, initially occupying the volume δV_0 , impinging on a force centre with momentum p_0 and impact parameter b . The vector δA is normal to the surface of area $b \delta b \delta \phi$. As time goes by, the volume changes to δV , and the momentum to p .

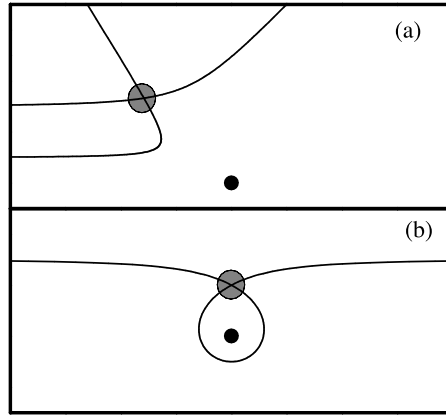


Figure 2. (a) There are two impact trajectories passing through the shaded point (r, θ) . (b) The control volume passes through (r, θ) at two different times.

reads

$$n_0 = \frac{\delta N}{\delta V_0} = \frac{jm}{p_0}. \quad (2)$$

We follow the evolution of the fixed number of particles δN in the volume δV_0 . As these particles approach the force centre, the trajectories $\mathbf{r}(t)$ depart from equation (1). This variation gives rise to a spatial dependence of the volume δV . Thus, the particle density $n(\mathbf{r}) = \delta N/\delta V$ reads

$$n(\mathbf{r}) = \frac{\delta N}{\delta V} = \frac{\delta N}{\delta V_0} \frac{\delta V_0}{\delta V} = n_0 \left| \frac{\partial(\mathbf{r}_0)}{\partial(\mathbf{r})} \right|, \quad (3)$$

where $\partial(\mathbf{r}_0)/\partial(\mathbf{r})$ is the Jacobian of the transformation relating the trajectory $\mathbf{r}(t)$ and its asymptotic approximation $\mathbf{r}_0(t)$. Taking polar coordinates as shown in figure 1 and using the angular momentum conservation law, we obtain

$$n(\mathbf{r}) = n_0 \left| \frac{\partial(\mathbf{r}_0)}{\partial(\mathbf{r})} \right| = n_0 \frac{bp_0/m}{r^2 \sin \theta} \left| \frac{\partial(b, t)}{\partial(r, \theta)} \right|. \quad (4)$$

In order to evaluate this density, we need to know the impact parameter b defining the trajectory that crosses the point (r, θ) , and the time t when this crossing takes place. It should be noticed that the expressions $b = b(r, \theta)$ and $t = t(r, \theta)$ need not be single valued. In figure 2(a) we show a situation where there are two different trajectories reaching the same point in space. In this case, the function $b = b(r, \theta)$ has two branches. Similarly, figure 2(b) shows the case of a bivaluated $t = t(r, \theta)$ function. We therefore write

$$n(\mathbf{r}) = n_0 \frac{bp_0/m}{r^2 \sin \theta} \sum \left| \frac{\partial(b, t)}{\partial(r, \theta)} \right|, \quad (5)$$

where the sum runs over all the possible values of b and t corresponding to each point (r, θ) .

Since we are under stationary flux conditions, it should be possible to eliminate all explicit dependence on the time variable t . The existence of well defined time-independent trajectories implies that we can define any of two functions $r = r(b, \theta)$ and $\theta = \theta(b, r)$ relating the spatial coordinates and the impact parameter. Operating with the first or second relation we obtain

$$n(\mathbf{r}) = n_0 \frac{p_0/m}{r^2 \sin \theta} \sum \left| \frac{b}{\bar{\theta}} \left(\frac{\partial b}{\partial r} \right)_\theta \right|, \quad (6)$$

$$n(r) = n_0 \frac{p_0/m}{r^2 \sin \theta} \sum \left| \frac{b}{\dot{r}} \left(\frac{\partial b}{\partial \theta} \right)_r \right|, \quad (7)$$

respectively, where the sums run over all the contributions to the density. The derivatives $\dot{\theta} = (\partial\theta/\partial t)_b$ and $\dot{r} = (\partial r/\partial t)_b$ are calculated from angular momentum and energy conservation

$$|\dot{\theta}| = \frac{b p_0}{m r^2}, \quad |\dot{r}| = \frac{1}{m} \sqrt{p_0^2 - 2mV(r) - (b p_0/r)^2}. \quad (8)$$

Equations (6) and (7) provide two alternative methods for the calculation of the particle density in a collision problem. In order to compute $n(r)$, the relation $b = b(r, \theta)$ is needed, which we obtain by inverting the equation for the trajectory $r = r(b, \theta)$. In some cases, $b(r, \theta)$ may be a very complicated function of its arguments. In figure 3 we show the function b with the corresponding trajectories for the scattering by the dipolar potential $V(r) = \alpha/r^2$. In the attractive case ($\alpha < 0$), when the impact parameter b is smaller than r_D , with $r_D = (2m|\alpha|)^{1/2}/p_0$, the particle falls down to the force centre. For b slightly above r_D , the trajectories show orbiting, that is, they encircle the potential centre several times. We show the surface $b = b(r, \theta)$ in logarithmic scale for $b > r_D$. There is an infinite number of sheets accumulating at $b = b_0$. In the repulsive case ($\alpha > 0$), there are two different trajectories (i.e. two impact parameters) passing through each point (r, θ) (except for $\theta = \pi$). All these branches of $b = b(r, \theta)$ contribute to the sums in (6) and (7).

Besides, if a single trajectory passes through a given point (r, θ) more than once (see figure 2(b)), the surface $b(r, \theta)$ shows a crossing of two of its branches, as shown in figure 3(a) for the dipolar potential. Only one impact parameter is associated to each point (r, θ) at the crossing, but there is more than one derivative $(\partial b/\partial r)_\theta$ or $(\partial b/\partial \theta)_r$. Again, there are several contributions to the sums in (6) and (7).

It may also happen that there is no trajectory reaching a given point (r, θ) . We are therefore in the presence of a *shadow zone*, or *forbidden region* where the spatial density is strictly zero. Figure 3(b) shows an example of this situation for the potential $V(r) = \alpha/r^2$ ($\alpha > 0$).

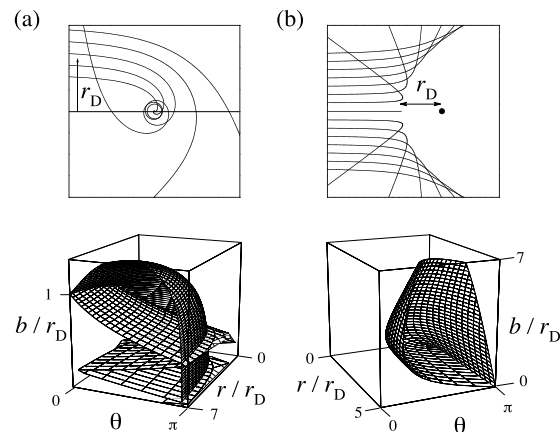


Figure 3. Impact parameter b as a function of the spatial coordinates (r, θ) , with the corresponding trajectories. The potential is $V(r) = \alpha/r^2$. In (a) we depict the attractive case ($\alpha < 0$). Trajectories with $b < r_D$ fall towards the force centre. The function $b(r, \theta)$ is plotted in logarithmic scale, for $b > r_D$. The surface shows an infinite number of foldings, as $b \rightarrow r_D$. In (b) we depict the repulsive case ($\alpha > 0$). The absence of particles in the neighbourhood of the force centre implies that the function $b(r, \theta)$ is not defined for $r \approx 0$.

Finally, there are a number of situations that give rise to a high concentration of particles at a given point (r, θ) . For instance, it may happen that $\sin \theta = 0$, while $|\partial(b, t)/\partial(r, \theta)| \neq 0$ in (4), leading to a divergence of the density in the forward or backward directions. This phenomenon is similar to the *glory caustic* in geometrical optics. In figure 4(a) we show how the particles that are initially distributed on a two-dimensional annular ring are squeezed into a line segment when crossing the $\theta = 0$ axis.

It can also happen that the Jacobian $|\partial(b, t)/\partial(r, \theta)|$ diverges. By angular momentum conservation, the angular velocity $\dot{\theta}$ in (6) cannot vanish. Thus, a divergence in the Jacobian can only occur when $(\partial b/\partial r)_\theta = \infty$. This condition is fulfilled on a curve $r = r(\theta)$ where the surface $b = b(r, \theta)$ is vertical (the outermost part of the surface in figure 3(b)). In other words the trajectories accumulate on a surface of revolution (defined by the curve $r(\theta)$), which is touched tangentially by the beam. Due to its similarity with the optical phenomenon, we interpret this divergence as a *rainbow caustic*. In figure 4(b) we show an example of this situation for the cut-off Coulomb potential $V(r) = Z(1/R - 1/r)$ if $r < R$ and $V(r) = 0$ for $r \geq R$. There is a complex structure of caustics, even though the potential is a fairly simple one.

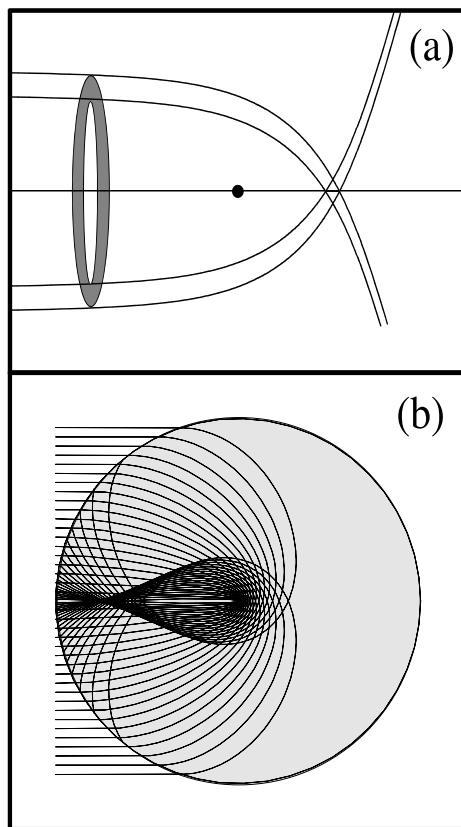


Figure 4. (a) The particles that are initially distributed in a two-dimensional annular ring are grouped together on a one-dimensional line segment, when crossing the polar axis. There, the density diverges, producing a glory effect. (b) Beam of trajectories for the cut-off Coulomb potential $V(r) = (-Z/r + Z/R)H(R - r)$, where H is the Heaviside step function. The shaded region represents the sphere $r \leq R$. There is a complicated structure of rainbow caustics, where trajectories accumulate.

In the asymptotic region, the quantum mechanical stationary wavefunction can be separated into incoming and outgoing terms. A similar separation can be made in our classical description, identifying an incoming, an outgoing, and eventually, one or more halfway contributions to the spatial density. Such a classification is given naturally by the different branches of the function $b = b(r, \theta)$ in equations (6) and (7). For instance, in figure 3(b) we identify two branches, separated by the rainbow caustic $r = r(\theta)$ where the derivatives $\partial b/\partial r$ and $\partial b/\partial \theta$ diverge. In the case where there is orbiting (as in figure 3(a)) the surface has to be unfolded by allowing θ to vary between $-\infty$ and $+\infty$. Branch m is defined as the unfolded surface between $\theta = m\pi$ and $(m+1)\pi$.

Each particle of the test volume of figure 1 follows an orbit defined by the intersection of the surface $b = b(r, \theta)$ and a horizontal plane $b = \text{constant}$. In doing so, it moves naturally from one sheet to another. It is clear that the sheet containing the test volume long before the collision corresponds to an incoming contribution $n_+(r)$. Similarly, the last branch visited by the particles gives the outgoing contribution $n_-(r)$. All the sheets in between can be classified as halfway ones.

Just as in the quantum mechanical description, the scattering cross section can be obtained from the normalized density at infinity. By definition, $\sigma(\Theta)$ is the number of particles passing through a surface far away from the force centre, per unit time, solid angle, and incident flux. In terms of the particle distribution $n(r)$, it reads (Fiol *et al* 1997)

$$\sigma(\Theta) = \lim_{r \rightarrow +\infty} \frac{r^2}{n_0} n_-(r, \Theta), \quad (9)$$

where $n_-(r)$ is the outgoing density. Using equation (7), and considering that $\lim_{r \rightarrow +\infty} \dot{r} = p_0/m$, we recover the definition of the cross section

$$\sigma(\Theta) = \frac{1}{\sin \Theta} \sum_b b \left| \frac{db}{d\Theta} \right|. \quad (10)$$

Here, the angle Θ is defined as the limiting value of θ , for $r \rightarrow +\infty$.

3. The density in momentum space

Under stationary flux conditions, there is a well defined momentum field $\mathbf{p} = \mathbf{p}(r)$. Hence, the probability $\tilde{n}(\mathbf{p})$ of finding a particle with momentum in a region $d\mathbf{p}$ around \mathbf{p} reads

$$\tilde{n}(\mathbf{p}) = n(r) \left| \frac{\partial(r)}{\partial(\mathbf{p})} \right| = n_0 \left| \frac{\partial(\mathbf{r}_0)}{\partial(r)} \frac{\partial(r)}{\partial(\mathbf{p})} \right| = n_0 \left| \frac{\partial(\mathbf{r}_0)}{\partial(\mathbf{p})} \right|. \quad (11)$$

We are assuming that each reachable momentum \mathbf{p} can be traced back at most, to a finite number of initial asymptotic states $\mathbf{r}_0(t)$. This seems to be a very permissive condition. However it rules out simple situations such as any cut-off potential, where the initial momentum is related to an infinite number of impact parameters. These cases have to be considered on an individual basis.

Taking polar coordinates and using the angular momentum conservation law, we obtain

$$\tilde{n}(\mathbf{p}) = n_0 \frac{bp_0/m}{p^2 \sin \theta_p} \left| \frac{\partial(b, t)}{\partial(p, \theta_p)} \right|. \quad (12)$$

This relation is completely analogous to equation (4) in coordinate space. Following the same line of reasoning as in the previous section, we obtain

$$\tilde{n}(\mathbf{p}) = n_0 \frac{p_0/m}{p^2 \sin \theta_p} \sum \left| \frac{b}{\dot{\theta}_p} \left(\frac{\partial b}{\partial p} \right)_{\theta_p} \right|, \quad (13)$$

$$\tilde{n}(\mathbf{p}) = n_0 \frac{p_0/m}{p^2 \sin \theta_p} \sum \left| \frac{b}{\dot{p}} \left(\frac{\partial b}{\partial \theta_p} \right)_p \right|, \quad (14)$$

where the sum covers all the possible contributions to the density at (p, θ_p) . These equations provide two alternative methods to calculate the particle distribution in momentum space. Formally, they are equivalent to equations (6) and (7) in coordinate space. Just as before, an expression of the function $b(p, \theta_p)$ is needed.

Energy and angular momentum conservation imply

$$|\dot{p}| = |V'(r)| \sqrt{1 - \left(\frac{b p_0}{r p} \right)^2}, \quad |\dot{\theta}_p| = \frac{b p_0}{r p^2} |V'(r)|, \quad (15)$$

where the relation $r = r(p)$ is obtained by the inverse of the potential energy

$$r(p) = V^{-1} \left(\frac{p_0^2 - p^2}{2m} \right). \quad (16)$$

Therefore, if $V(r)$ is not one-to-one, both $\dot{\theta}_p$ and \dot{p} are multivaluated functions.

It is clear from energy conservation that if the potential energy is bounded from below ($V(r) > V_{\min}$), the momentum p is bounded from above ($p < p_{\max} = \sqrt{p_0^2 - 2mV_{\min}}$). In this case, all the trajectories in momentum space are inside a sphere of radius p_{\max} . Outside this sphere, the function $b = b(p, \theta_p)$ is not defined and the density vanishes. Similarly, if the potential is bounded from above ($V(r) < V_{\max}$), the density is zero for all $p < p_{\min} = \sqrt{p_0^2 - 2mV_{\max}}$.

In a scattering process, all particles have initially the same momentum p_0 . Long before they reach the collision region, the effect of the force centre is negligible. Thus, initially they all travel an infinite amount of time before a significant variation in their momenta takes place. Therefore, the momentum distribution always diverges at $\mathbf{p} = \mathbf{p}_0$.

Similarly, long after the collision, the particles approach asymptotically their final momentum \mathbf{p}_f . Because of energy conservation, $|\mathbf{p}_f| = p_0$. Thus, outgoing particles spend an infinite amount of time near the surface of a sphere of radius p_0 . In consequence, on this sphere the density also diverges. Mathematically,

$$\lim_{p \rightarrow p_0} \dot{p} \tilde{n}_-(\mathbf{p}) = \frac{n_0}{m p_0} \lim_{p \rightarrow p_0} \frac{b_-}{\sin \theta_p} \left(\frac{\partial b_-}{\partial \theta_p} \right)_p = \frac{n_0}{m p_0} \sigma(\theta_p), \quad (17)$$

where \tilde{n}_- and b_- correspond to the outgoing density and impact parameter, respectively. Since \dot{p} vanishes for $p \rightarrow p_0$, the asymptotic density in equation (17) always shows a divergence. On the sphere $|\mathbf{p}| = p_0$, the scattering cross section gives the angular dependence of \tilde{n} .

4. The perfectly rigid sphere

A beam of particles of mass m and momentum p_0 is elastically reflected at the surface of a perfectly rigid sphere of radius a , as shown in figure 5. Each orbit is made of two straight lines, corresponding to two different sheets of the function $b = b(r, \theta)$. While the branch associated to the incoming trajectories is simply given by $b_+ = r \sin \theta$, the one associated to the outgoing trajectories reads

$$b_- = a \sin \beta(r, \theta), \quad (18)$$

where the angle β between the incoming trajectory and the normal to the sphere at the point of reflection (see figure 5(a)) is related to the point (r, θ) by the implicit equation

$$r \sin(\theta + 2\beta) + a \sin \beta = 0. \quad (19)$$

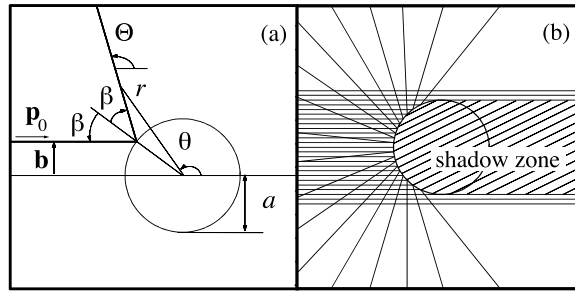


Figure 5. (a) A trajectory is reflected on the surface of a rigid sphere. (b) The beam of particles scatters from a rigid sphere. Only those trajectories with $b < a$ are deflected. Behind the sphere there is a shadow zone.

We note that the impact parameters b_- for these outgoing trajectories are always smaller than the radius of the sphere. Furthermore, these equations hold only outside the *shadow zone* in figure 5(b). These expressions can be used to evaluate the particle density as a sum of two terms, $n(\mathbf{r}) = n_+(\mathbf{r}) + n_-(\mathbf{r})$, with $n_+(\mathbf{r}) = n_0$ and

$$n_-(r, \theta) = n_0 \left| \frac{\sin^2(\theta + 2\beta) \cos \beta}{\sin \theta [\cos \beta \sin(\theta + 2\beta) - 2 \sin \beta \cos(\theta + 2\beta)]} \right|, \quad (20)$$

where $\beta = \beta(r, \theta)$ is given by equation (19). Both equations are only valid outside the shadow zone. In figure 6(a) the incoming and the outgoing classical particle distributions are shown. The well known expression for the differential cross section of the rigid sphere is readily obtained as the asymptotic limit of the outgoing density

$$\sigma(\Theta) = \lim_{r \rightarrow +\infty} r^2 \frac{n_-(r, \Theta)}{n_0} = \frac{a^2}{4}. \quad (21)$$

Let us now compare these results with the quantum mechanical particle distribution $|u(r, \theta)|^2$, where the wavefunction $u(r, \theta)$, normalized to an incoming density equal to n_0 , reads (Schiff 1965)

$$u(r, \theta) = u_+(r, \theta) + u_-(r, \theta), \quad (22)$$

with

$$\begin{aligned} u_+(r, \theta) &= \sqrt{n_0} \sum_{\ell=0}^{+\infty} (2\ell + 1) i^\ell j_\ell(p_0 r / \hbar) P_\ell(\cos \theta), \\ u_-(r, \theta) &= \sqrt{n_0} \sum_{\ell=0}^{+\infty} (2\ell + 1) i^\ell \left[(e^{i\delta_\ell} \cos \delta_\ell - 1) j_\ell(p_0 r / \hbar) - e^{i\delta_\ell} \sin \delta_\ell \eta_\ell(p_0 r / \hbar) \right] P_\ell(\cos \theta). \end{aligned} \quad (23)$$

Here, P_ℓ , j_ℓ and η_ℓ stand for the Legendre polynomial and the spherical regular and irregular Bessel function, respectively. The phase shift δ_ℓ reads

$$\delta_\ell = \arctan \left[\frac{j_\ell(p_0 a / \hbar)}{\eta_\ell(p_0 a / \hbar)} \right]. \quad (24)$$

The quantum mechanical distributions arising from the square moduli of u_+ , u_- and u are depicted in figure 6(b). Outside the shadow zone, the incoming and outgoing densities show the same qualitative behaviour as the corresponding classical distributions. In contrast, $|u|^2$ shows a complicated oscillatory structure which is not present in the classical result. Clearly, this is an interference process between the two smooth incoming and outgoing amplitudes. The

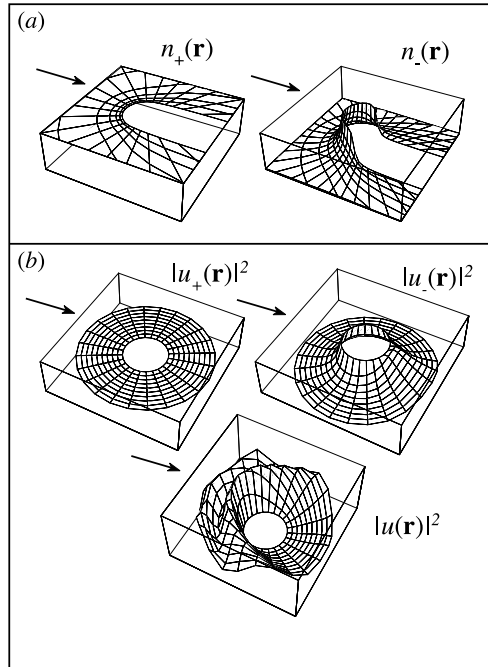


Figure 6. (a) Classical incoming (n_+) and outgoing (n_-) densities for scattering on a rigid sphere. (b) Quantum mechanical incoming ($|u_+|^2$), outgoing ($|u_-|^2$) and total ($|u|^2$) particle distributions. Outside the shadow zone, the partial classical and quantum mechanical densities behave qualitatively the same. The total distributions, however, differ significantly, since the quantum mechanical approach shows an oscillatory interference structure.

wavelength of the oscillations increases with $\lambda = 2\pi\hbar/p_0$. Due to a diffraction phenomenon, the total quantum mechanical distribution does not vanish in the shadow zone, except at the limit $\lambda/a \rightarrow 0$. Nevertheless, not even in this classical limit does the outgoing density reach a small value in the forbidden region. In order to have a small total probability of finding particles in the shadow zone, the square modulus of u^- must remain close to the square modulus of u^+ , and the phases of both functions should be opposite.

Let us finally turn to momentum space. Long before a particle reaches the sphere, its momentum remains fixed at $\mathbf{p} = \mathbf{p}_0$. As the result of an impulsive force at the surface of the sphere, this momentum jumps to some other value \mathbf{p}_f , where it remains thereafter. It is clear that this pathological process cannot be treated within the present framework (equation (14)), except as the limiting case of a smooth potential. Because of energy conservation, $|\mathbf{p}_f| = p_0$ and the particle density in momentum space is different from zero (actually diverges) only on the surface of a sphere of radius p_0 .

5. Rutherford scattering

We now analyse the spatial density in the Rutherford problem, first treated by Gordon (1928). We consider the potential $V(r) = Z/r$, and apply the methods derived above.

The equation of a trajectory with impact parameter b reads

$$\frac{b}{r} = -\frac{r_C}{b} \frac{1 + \cos \theta}{2} + \sin \theta, \quad (25)$$

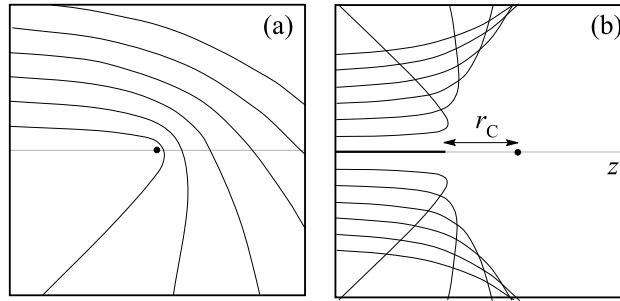


Figure 7. Trajectories encountered in the Rutherford scattering, for (a) an attractive, and (b) repulsive potential. The initial momentum is parallel to the z axis.

with

$$r_C = \frac{Z}{p_0^2/2m}. \quad (26)$$

In figure 7 we show the beam of trajectories for the attractive ($Z < 0$) and repulsive ($Z > 0$) cases. We readily see that in this latter case there is a shadow zone limited by a rainbow caustic at the paraboloid

$$\frac{r}{r_C} \frac{1 - \cos \theta}{2} = 1, \quad (27)$$

defined by $(\partial r / \partial \rho)_\theta = 0$. On the other hand, when the potential is attractive, every point in coordinate space is reached by the beam of trajectories. This includes the forward direction $\theta = 0$, where a glory caustic occurs.

Equation (25) can be inverted, to obtain the impact parameter b as a function of the spatial coordinates (r, θ)

$$b_\pm = \frac{r \sin \theta}{2} \left(1 \pm \sqrt{1 - \frac{2r_C}{r} \frac{1}{(1 - \cos \theta)}} \right), \quad (28)$$

where b_+ and b_- correspond to the incoming and outgoing trajectories.

Using equation (6) or (7) to calculate the spatial density, we obtain

$$n(\xi) = n_+(\xi) + n_-(\xi), \quad (29)$$

with

$$n_\pm(\xi) = \frac{n_0}{4} \frac{(1 \pm \sqrt{1 - 1/\xi})^2}{\sqrt{1 - 1/\xi}} H[\xi(\xi - 1)], \quad (30)$$

where H stands for the Heaviside step function[†]. We see that the classical density is a function of the coordinates (r, θ) only in the combination

$$\xi = \frac{r}{r_C} \frac{1 - \cos \theta}{2} = \frac{1}{2p_0 r_C} (p_0 r - \mathbf{p}_0 \cdot \mathbf{r}). \quad (31)$$

This parameter is positive for a repulsive potential and negative for an attractive one. The forward direction $\theta = 0$ corresponds to $\xi = 0$. A constant value of $|\xi|$ defines a paraboloid with *perihelion* $r_o = \xi r_C$. The vanishing of the step function for $0 < \xi < 1$ and the

[†] $H(x) = 1$ if $x > 0$, and $H(x) = 0$, if not.

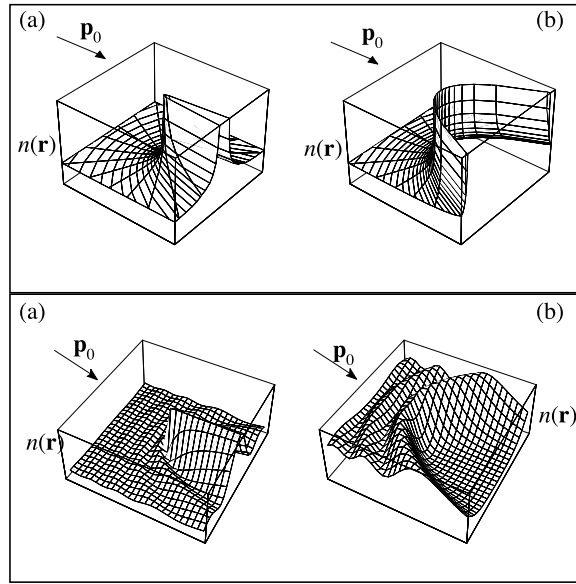


Figure 8. Particle density in coordinate space for an (a) attractive and (b) repulsive Coulomb potential. Upper part: classical description, lower part: quantum mechanical description.

divergencies at $\xi = 0$ and $\xi = 1$ account for the shadow zone and the glory and rainbow caustics, respectively.

Both the partial densities n_{\pm} and the total one

$$n(\xi) = n_0 \frac{1 - 1/2\xi}{\sqrt{1 - 1/\xi}} H[\xi(\xi - 1)], \quad (32)$$

comply with

$$n(\xi) = n(1 - \xi), \quad (33)$$

relating the density at one point in space with the density in some other place, with the opposite sign of the potential. It has long been known that the asymptotic particle distribution (i.e. the cross section) does not depend on the sign of the potential. This relation represents an extension of this property to the whole coordinate space. In the upper part of figure 8 we show the classical density (32) in (a) the attractive and (b) the repulsive cases.

Taking the limit $|\xi| \rightarrow +\infty$ we obtain

$$\lim_{|\xi| \rightarrow \infty} n_{-}(\xi) = \frac{n_0}{(4\xi)^2} + \dots \quad (34)$$

Thus, the Rutherford cross section reads

$$\sigma(\Theta) = \lim_{r \rightarrow +\infty} r^2 \frac{n_{-}(r, \Theta)}{n_0} = \frac{(r_C/4)^2}{\sin^4(\Theta/2)}. \quad (35)$$

We now compare our results with the quantum mechanical particle distribution $n = |\Psi_{p_0}(\mathbf{r})|^2$, where

$$\Psi_{p_0}(\mathbf{r}) = \sqrt{n_0} e^{-\pi v/2} \Gamma(1 + iv) e^{ip_0 \cdot \mathbf{r}/\hbar} {}_1F_1[-iv; 1; i(p_0 r - \mathbf{p}_0 \cdot \mathbf{r})/\hbar] \quad (36)$$

is the stationary Coulomb wavefunction. Similarly to the classical situation, the particle distribution

$$n(v, \xi) = n_0 \frac{2\pi v}{e^{2\pi v} - 1} |{}_1F_1(1 + iv; 1; -4iv\xi)|^2 \quad (37)$$

depends on the spatial coordinates only through the reduced variable ξ . However, it contains an extra dimensionless parameter

$$\nu = \frac{Zm}{\hbar p_0}, \quad (38)$$

dependent on \hbar . The size of this parameter is a measure of the validity of the classical approach.

In the lower part of figure 8 we see that the rainbow and glory divergences of the classical approach appear now as finite maxima. The location of these maxima has a similar dependence on the parameters Z , m and p_0 as the corresponding divergences in the classical density. In the forward direction, the density

$$n(\nu, 0) = n_0 \frac{2\pi\nu}{e^{2\pi\nu} - 1} \quad (39)$$

diverges for an attractive potential ($\nu < 0$) and vanishes in the repulsive case ($\nu > 0$) for $\hbar \rightarrow 0$. Thus, the classical behaviour is recovered. However, for a finite \hbar , the classical shadow region is not strictly forbidden due to a diffraction phenomenon. In figure 9 we show a quantitative comparison between the classical and the quantum mechanical densities in coordinate space. The attractive case corresponds to $\xi \in (-\infty, 0]$, and the repulsive one, to $\xi \in [0, +\infty)$.

For a small $\nu\xi$, we use the stationary phase method (Samengo 1998b) to approximate the stationary Coulomb wavefunction as

$$\Psi_{p_0}(r) \rightarrow \sqrt{n_+(\xi)}e^{iS_+/\hbar} + \sqrt{n_-(\xi)}e^{iS_-/\hbar}, \quad (40)$$

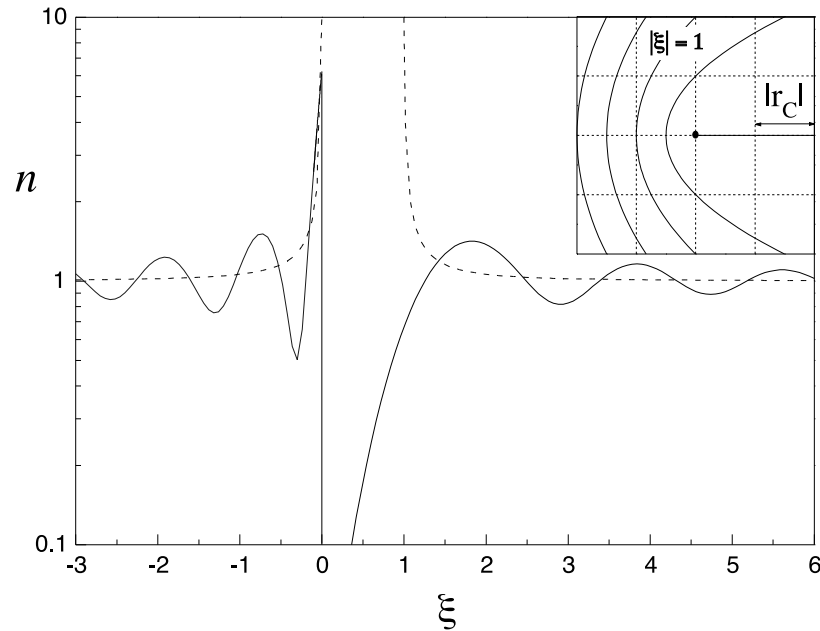


Figure 9. Quantitative comparison between the classical (---) and the quantum mechanical (—) particle density in coordinate space for an attractive ($\nu = -1$, $\xi \in (-\infty, 0]$) and repulsive ($\nu = 1$, $\xi \in [0, +\infty)$) Coulomb potential. Insert: geometrical place corresponding to fixed values of the reduced variable $|\xi|$.

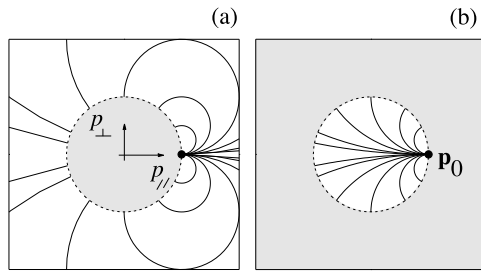


Figure 10. Trajectories in momentum space for (a) an attractive, and (b) a repulsive Coulomb potential. Shaded areas correspond to forbidden zones.

where n_\pm are the classical densities, and

$$S_\pm = p_0 r \cos \theta + \frac{p_0 r_C}{2} \left[2\xi \left(1 \mp \sqrt{1 - 1/\xi} \right) + \ln \left(\frac{1 \pm \sqrt{1 - 1/\xi}}{1 \mp \sqrt{1 - 1/\xi}} \right) \right] \quad (41)$$

are the classical actions for the incoming or outgoing trajectories reaching the point r . This equation generalizes a result first obtained by Rowe (1987) for the attractive case. Taking the square modulus of equation (40) we obtain

$$n(v, \xi) = n_+(\xi) + n_-(\xi) + 2\sqrt{n_+(\xi)n_-(\xi)} \cos[S_+/\hbar - S_-/\hbar]. \quad (42)$$

Hence, the semiclassical distribution is the sum of the partial incoming and outgoing classical densities, plus an interference term that is responsible for the oscillations observed in figures 8 and 9. These oscillations are due to path interference between the indistinguishable incoming and outgoing trajectories. It may be shown that the amplitude of the last term in (42) does not vanish in the classical limit $|v| \rightarrow \infty$. However, the wavelength of the oscillations is proportional to $1/|v|$. Thus, when $\hbar \rightarrow 0$, the quantum mechanical particle density oscillates so fast that the classical result is recovered in average.

We now evaluate the particle density in momentum space. Each particle describes an arc of a circle of radius $r_C p_0/2b$, centred at $\mathbf{p}_0 + (r_C p_0/2b^2)\mathbf{b}$ (Sommerfeld 1964, Norcliffe 1975), and keeps either inside or outside the circle $p = p_0$ for the repulsive or attractive case, respectively (see figure 10). Using either equation (13) or (14), the momentum distribution is obtained. It reads

$$\tilde{n}(\mathbf{p}) = 2n_0 \left(\frac{|r_C|}{p_0} \right)^3 \left(\frac{p_0^2}{p_0^2 - p^2} \right)^2 \frac{p_0^4}{|\mathbf{p} - \mathbf{p}_0|^4} H[Z(p - p_0)], \quad (43)$$

where H stands for the Heaviside step function. The upper part of figure 11 shows the density in momentum space for (a) an attractive, and (b) a repulsive Coulomb potential. In both cases there is a divergence all along the circle $p = p_0$, as anticipated by equation (17).

We now compare the classical result with the quantum mechanical particle distribution $\tilde{n} = |\tilde{\Psi}_{p_0}(\mathbf{p})|^2$. The Fourier transform of $\Psi_{p_0}(\mathbf{r})$ reads (Barrachina and Macek 1989)

$$\tilde{\Psi}_{p_0}(\mathbf{p}) = \sqrt{n_0} (2\pi\hbar)^{3/2} \left\{ \gamma \frac{\Gamma(2 + i\nu)}{\pi^2 e^{\pi\nu/2}} \frac{[p^2 - (p_0 + i\gamma)^2]^{i\nu}}{[|\mathbf{p} - \mathbf{p}_0|^2 + \gamma^2]^{2+i\nu}} + \frac{\nu p_0}{[(p_0 + i\gamma) - p^2]} \frac{\Gamma(1 + i\nu)}{\pi^2 e^{\pi\nu/2}} \frac{[p^2 - (p_0 + i\gamma)^2]^{i\nu}}{[|\mathbf{p} - \mathbf{p}_0|^2 + \gamma^2]^{1+i\nu}} \right\}, \quad (44)$$

with γ a small and positive regularization parameter. The first term in this modified Lippmann–Schwinger equation is a Coulomb asymptotic state, as defined by van Haeringen (1976). It

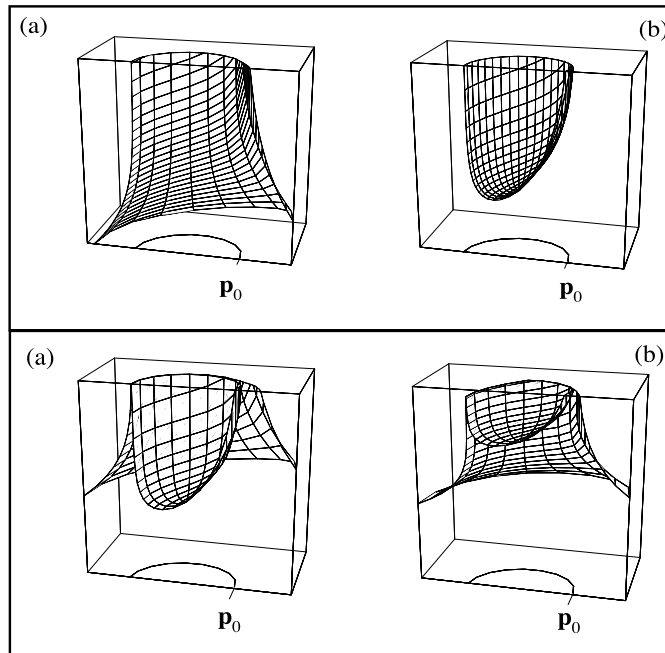


Figure 11. Particle density in momentum space for (a) an attractive, and (b) a repulsive Coulomb potential. Upper part: classical description, lower part: quantum mechanical description.

accounts for the divergence produced by the unscattered beam, with

$$\lim_{\gamma \rightarrow 0} \frac{\gamma/\pi^2}{[|\mathbf{p} - \mathbf{p}_0|^2 + \gamma^2]^2} = \delta(\mathbf{p} - \mathbf{p}_0). \tag{45}$$

Since our classical calculation does not include this limit, we shall exclude the forward direction ($\mathbf{p} = \mathbf{p}_0$) from our analysis. In the second term we recognize the free Green function multiplied by a regularized transition matrix element. Its square modulus reads

$$\tilde{n}(\mathbf{p}) = 2 n_0 \left(\frac{r_C}{p_0}\right)^3 \left(\frac{p_0^2}{p_0^2 - p^2}\right)^2 \frac{p_0^4}{|\mathbf{p} - \mathbf{p}_0|^4} \mathcal{S}_v(p - p_0), \tag{46}$$

where we have defined

$$\begin{aligned} \mathcal{S}_v(p - p_0) &= 2 \operatorname{sgn}(v) \frac{|\Gamma(1 + iv)|^2}{e^{\pi v}} \lim_{\gamma \rightarrow 0} |[p^2 - (p_0 + i\gamma)^2]^{iv}|^2 \\ &= \begin{cases} \operatorname{sgn}(v)(1 - e^{-2\pi v})^{-1} & \text{for } p < p_0 \\ \operatorname{sgn}(v)(e^{2\pi v} - 1)^{-1} & \text{for } p > p_0. \end{cases} \end{aligned} \tag{47}$$

We see that the classical and quantum mechanical expressions for $\tilde{n}(\mathbf{p})$ coincide, except for the Heaviside step function $H[Z(p - p_0)]$ which is replaced by $\operatorname{sgn}(r_C)\mathcal{S}_v(p - p_0)$. Both densities diverge at the sphere $p = p_0$. But now it is no longer true that the particles are either inside or outside the sphere, as shown in the lower part of figure 11. As in coordinate space, the quantum mechanical approach shows a nonvanishing probability of finding particles in regions that are

classically forbidden. This diffraction phenomenon is regulated by the function $\mathcal{S}_\nu(p - p_0)$ which coincides with the Heaviside step function in the classical limit $\nu \rightarrow \infty$

$$\lim_{\nu \rightarrow \infty} \mathcal{S}_\nu(p - p_0) = H[Z(p - p_0)]. \quad (48)$$

Hence, the classical expression is exactly recovered. Finally, we emphasize that in momentum space, trajectories do not cross (see figure 10). Thus, in contrast to what happens in coordinate space, no path interference can take place, and both the classical and the quantum mechanical densities show a smooth behaviour.

6. Conclusions

In this paper we have studied the classical scattering particle distributions, both in coordinate and momentum spaces. These distributions are produced by an ensemble of trajectories obeying the same restrictions imposed on the scattering solution of the Schrödinger equation. The classical density can be interpreted either as the particle distribution that actually builds up when a uniform beam of non-interacting particles collides with a force centre, or as an abstract construction resulting from an ensemble of individual scattering events.

The classical density is calculated by summing together the contributions of individual trajectories. This represents an important difference from the quantum mechanical approach, in which only amplitudes can be added together. The total density is then calculated by taking the square modulus of the total amplitude. This methodological discrepancy is a consequence of a fundamental difference between classical and quantum mechanics. As a result, classical densities lack the oscillatory structures often found in the quantum mechanical approach. Nevertheless, even when these differences are found, our classical method provides a useful tool to identify the several contributions that are interfering.

In this paper, coordinate and momentum spaces are treated on an equal footing. Although by intuition the process under study is usually described in coordinate space, the analysis in momentum space is just as important, since many of the calculations in quantum collision theory are made in the momentum representation. Therefore, if a classical reference is needed, it is important to have in mind the purely classical momentum distribution. For instance, it is well known that the classical and quantum expressions for the Rutherford scattering cross section are identical. Here we have shown that the same is valid for the square modulus of the Coulomb wavefunction in momentum space, except for a multiplying distortion factor that, in the classical limit, converges to a Heaviside step function related to the conservation of energy.

We propose that our general expression for the classical distribution may serve to guide semiclassical approximations of the transition matrices as well as to visualize the quantum mechanical particle distributions. For example, when making an eikonal approximation of the transition matrix in ionization or capture processes, the continuum wavefunction is replaced by a phase factor. In this way, the asymptotic conditions are described properly. However, when this is done, no care is taken to analyse if such a replacement produces a significant modification in the particle distribution in the neighbourhood of the collision region. We suggest that $\sqrt{n(\mathbf{r})} \exp(iS(\mathbf{r})/\hbar)$ represents a much better alternative for a semiclassical approximation.

In this paper we have shown that the classical density is well defined, and may be easily computed. The calculation itself throws light on the identification of relevant physical processes, as rainbow or glory effects. We propose that the comparison between the classical and the quantum mechanical particle densities may be useful to characterize and enrich the analysis of a collision process.

Acknowledgment

Partial support by the Agencia Nacional de Promoción Científica y Tecnológica (Programa de Modernización Tecnológica, Contrato de Préstamo BID 802 OC-AR) is gratefully acknowledged.

References

- Barrachina R O and Macek J H 1989 *J. Math. Phys.* **30** 2581
Berry M V and Mount K E 1972 *Rep. Prog. Phys.* **35** 315–97
Brink D M 1985 *Semi-classical Methods in Nucleus–Nucleus Scattering* (Cambridge: Cambridge University Press)
Fiol J, Pregliasco R G, Samengo I and Barrachina R O 1997 *Am. J. Phys.* **65** (2) 1–4
Fock V 1935 *Z. Phys.* **98** 145
Ford K W and Wheeler J A 1959a *Ann. Phys., NY* **7** 259–86
Ford K W and Wheeler J A 1959b *Ann. Phys., NY* **7** 287–322
Goldstein H 1959 *Classical Mechanics* (London: Addison-Wesley)
Gordon W 1928 *Z. Phys.* **48** 180–91
Gryzinski M 1965 *Phys. Rev. A* **138** 323
Gutzwiller M C 1967 *J. Math. Phys.* **8** 1979–2000
Landau L D and Lifshitz E M 1976 *Mechanics* (Oxford: Pergamon)
Mapleton R A 1966 *Proc. Phys. Soc.* **87** 219
McDowell M R C and Coleman J P 1970 *Introduction to the Theory of Ion-Atom Collisions* (Amsterdam: North Holland)
Norcliffe A 1975 *Case Stud. At. Phys.* **4** 1–55
Pitaevskii L P 1962 *Sov. Phys.–JETP* **15** 919
Reinhold C O, Schultz D R, Olson R E, Kelbch C, Koch R and Schmidt-Böcking H 1991 *Phys. Rev. Lett.* **66** 1842
Rowe P 1987 *J. Phys. A: Math. Gen.* **20** 1419
Samengo I 1998a *Phys. Rev. A* **58** 2767
——— 1998b *Phys. Rev. A* **58** 5001
Schiff L I 1965 *Quantum Mechanics* ch 5 (New York: McGraw-Hill)
Sommerfeld A 1964 *Mechanics* (New York: Academic)
Swenson J K and Burgdörfer J 1991 *Phys. Rev. Lett.* **66** 417–20
van Haeringen H 1976 *J. Math. Phys.* **17** 995